Optical-to-microwave frequency conversion with Rydberg excitons

David Ziemkiewicz* and Sylwia Zielińska-Raczyńska
Institute of Mathematics and Physics, Technical University of Bydgoszcz, and Al. Prof. S. Kaliskiego 7, 85-789 Bydgoszcz, Poland

(Received 8 February 2023; revised 8 May 2023; accepted 12 May 2023; published 22 May 2023; corrected 6 March 2025)

A copper-based plasmonic system is presented to provide optical-to-microwave photon conversion. The process uses highly excited levels in Cu_2O Rydberg excitons and takes advantage of spoof plasmons, which allow for significant enhancement of the transition probability between specific excitonic energy levels. The theoretical results are verified with numerical simulations. The proposed system is very flexible, allowing for emission of microwave wavelengths from 0.1 to 10 mm.

DOI: 10.1103/PhysRevB.107.195303

I. INTRODUCTION

The process of optical frequency conversion provides a fundamental and important approach to modify light in the frequency domain. Possibilities of manipulating the frequency without changing the information of other degrees of freedom of light will enable one to establish an interface between various optical systems operating in different frequency regions and have many classical and quantum applications [1,2]. Photons play an important role in quantum information science because they are excellent carriers of quantum information. A variety of quantum qubit systems exploiting excitations at optical frequencies or superconducting qubits operating at microwave frequencies have been described and practically applied [3,4]. However, optical photons can easily propagate over large distances, while microwave photons can be easily controlled in relatively macroscopic circuits [1]. Hence, designing photonic transducers, an important factor which must be considered, is an interplay between benefits and disadvantages, inherent in their physical character. Different components for a synchronic photon generation and manipulation in practical systems cannot interact directly due to the wavelength and frequency mismatch; thus, interfaces are needed to overcome such problems. A photon frequency interface capable of converting frequencies and bandwidths is indispensable. Improved coupling between optical and microwave frequencies would enhance classical telecommunications and would be applied in distributed quantum networks and quantum communication.

The first step toward many microwave applications is an efficient conversion of energy from optical frequencies to microwave ones. One of the techniques involves accelerating surface charge carriers in a semiconductor with a femtosecond laser [5–7], but this method results in a very short emission time and correspondingly wide emission spectrum; for example, an emission spectrum ranging from 0.1 to 7.5 THz is reported in Ref. [6]. This limitation also applies to terahertz emission from structured metallic surfaces [8] and photoconductor-based systems [9,10]. Our proposal can operate under continuous illumination and is tied to the spectral width of specific excitonic level transitions, which can vary from gigahertz to megahertz [11], making them significantly more narrowband. Another way of coupling is the use of Rydberg states of atoms placed in a cavity [12], but this approach demands a vacuum chamber and cryogenic cooling. In this paper, we propose the use of the solid-state analog of Rydberg atoms: Rydberg excitons (REs) in Cu_2O interacting with plasmons for the purpose of frequency conversion.

An exciton in a semiconductor is a quasiparticle consisting of a conduction band electron and a valence band hole bound by the Coulomb interaction. As a whole, it is an electrically neutral particle with many properties similar to a hydrogen atom. REs are the states characterized by a large principal quantum number and share many properties with Rydberg atoms. Excitonic states in Cu_2O with principal quantum numbers up to $n = 25$ have been observed [13]. Since then, this area of study has developed rapidly; right now, many groups focus on exploring the properties of REs in low-dimensional systems [14–17] and fabrication techniques of Cu_2O nanostructures [18,19]. Highly excited resonances in a RE Cu_2O system are very close to each other; they are separated by several millielectronvolts, which situates these transitions in the microwave region and allows for controlled emission of microwaves [20]. This makes Cu_2O a very promising candidate for solid-state microwave devices such as masers [21]. We proposed a continuous-mode solid-state maser based on Cu_2O in which an ensemble of highly excited RE states serves as a gain medium [21]. It was shown that the system is highly tunable with an external electric field, allowing for a wide range of emission frequencies within the terahertz range [11]. In contrast with these works, where a resonant cavity has been used as a device for enhancing the probability of specific microwave transitions, here, we focus on plasmonic structures and plasmon-exciton interactions due to their advantages in miniaturization and ease of fabrication [22,23]. Moreover, we do not rely on the nonlinear properties of the system, which is the basis of many conversion schemes [24–26]; these

*david.ziemkiewicz@utp.edu.pl

solutions tend to have relatively low efficiency, photon emission rate on the order of 10^4 per second [25], and need sufficient power to take advantage of the nonlinear properties.

Plasmons are a combination of light and a collective oscillation of the free electron plasma at the metal-dielectric interface. Surface plasmon polaritons (SPPs) can be described as dual waves of charge motion in a metal and electromagnetic (EM) waves in the surrounding medium. In general, it has been demonstrated that one can efficiently couple plasmons with excitons, forming so-called plexcitons [27,28], which have been proposed as the basis of a variety of tunable devices [29–31]. Usually, only plasmons in the infrared (IR)-visible-ultraviolet (UV) range are considered, which are chosen to match the energy of specific excitonic states [22]. However, for microwave inter-excitonic transitions, one has to take advantage of the so-called spoof plasmons [32], which are surface EM waves in the microwave and terahertz regimes; they propagate along planar interfaces with sign-changing permittivities. Since surface plasmons cannot appear naturally in microwave and terahertz frequencies due to dispersion properties of metals, spoof surface plasmons require artificially engineered materials [33–36]. Finally, we note that a Cu nanostructure can match the plasmon lifetime of the more traditional materials such as silver or gold [37,38], especially when coupled to a controlled layer of oxide [39,40]. Therefore, the use of the Cu-Cu_2O nanostructure provides multiple advantages: Direct coupling to Cu_2O excitons, low plasmonic energy loss, and ease of fabrication [41–43]. Moreover, the terahertz radiation can be either emitted as free space photons with the use of the coupling structure or kept in the form of surface plasmons, which is a particularly valuable option due to the lack of direct SPP sources in the terahertz regime [44].

This paper is organized as follows. In the first section, the theoretical descriptions of RE features, the Purcell effect, and spoof plasmons are outlined. Then the possibility of enhancing specific transition probabilities is analyzed theoretically and numerically, and the optimal system geometry is indicated. In the next section, the amplification factors are used to calculate the microwave emission power for specific excitonic transitions and to estimate conversion efficiency. The possibility of single-photon-level emission is also discussed. Finally, the conclusions are presented. The details of the numerical method used for field calculations are outlined in Appendix A.

II. THEORY

A. REs and Rydberg blockade

A RE is a highly excited electron-hole pair bound by Coulomb attraction, characterized by a principal quantum number $n \gg 1$ for dipole-allowed P-type envelope wave functions. In principle, REs have similar scaling as Rydberg atoms, although the physical origin of these similarities in their case is based on a complex valence band structure and different selection rules for excitons. The dimensions of REs scale as n^2 and can reach micrometers, and their lifetimes are proportional to n^3 and can reach hundreds of nanoseconds [13]. Another exceptional characteristic is their strong interaction with external fields due to the fact that their polarizability scales as n^7. In RE systems in copper oxide, electric dipole transitions in the microwave frequency region (10–1000 GHz) can be accessed with $n+1 \rightarrow n$ transitions, for $n > 8$. Interactions involving coupling of REs with microwaves have been observed recently in Cu_2O by Gallagher *et al.* [45], which confirms that the system of copper oxide with REs is a very promising candidate for solid-state microwave devices such as masers [21].

A significant feature of REs is Rydberg blockade, which results in long-range dipole-dipole and van der Waals interactions between them, which can be large enough to perturb the energy level of nearby excitons, so they no longer have the same frequency, which prevents their excitation in the immediate vicinity of an already existing exciton. The space where another exciton cannot be created is described by a so-called blockade volume, which scales extremely fast as n^7 [13]:

$$V_b \approx 3 \times 10^{-7}\,\mu\text{m}^3 \cdot n^7. \tag{1}$$

As a consequence, highly excited states very quickly reach the saturation level when the medium is completely filled with excitons. Thus, the light propagating through the medium is not absorbed to create new ones. In conclusion, the maximum number of excitons that can exist in any given volume is strictly limited. In the system presented below, this volume is the immediate vicinity of the proposed plasmonic structure. As will be shown later, aside from thermal considerations, Rydberg blockade is the main limiting factor on the microwave emission power.

B. Material model and system setup

In our previous papers describing the maser on REs, we proposed the use of a metallic cavity for enhancing the probability of microwave transitions [21]. However, such an approach has some limitations. The Cu_2O crystal that fills the cavity becomes inconveniently large in the case of longer wavelengths approaching 1 mm; for such a size, it becomes opaque for visible light, so an illuminating optical beam penetrates only the surface layer of the medium, up to the depth of a few tens of micrometers. Thus, only a small fraction of the crystal volume is occupied by excitons, which is an important limitation considering the large volume taken by excitons and the resulting Rydberg blockade.

An alternative approach, which allows us to overcome this limitation, is some sort of resonant, plasmonic structure that is surrounded by Cu_2O. A plasmonic structure capable of sustaining microwave plasmons was proposed by Pendry *et al.* [46] and had a form of thin, metallic wires. We recall that the electron plasma frequency is given by

$$\omega_p^2 = \frac{Ne^2}{\epsilon_0 m_e}, \tag{2}$$

where N is the charge carrier (electron) concentration, and m_e is the electron effective mass. For copper, the plasma frequency $\hbar\omega_p \approx 7.4$ eV, which corresponds to the ultraviolet spectral range. However, as shown by Pendry *et al.* [46], the effective mass of an electron can be greatly enhanced in a sufficiently thin wire, resulting in decreased plasma frequency. This effect can be attributed to the fact that an electron moving in a very thin wire generates significant magnetic field

in the limit of the wire radius $r \to 0$, which increases the inductance of the system. That additional inductance disturbs the acceleration of the electron and thus increases its apparent inertia, i.e., the effective mass, allowing for efficient coupling to microwave frequency radiation unlike the optical frequencies usually employed in plasmonics. This mechanism has been used to facilitate negative permittivity in experimentally demonstrated negative index metamaterials [47]. The type of microwave surface wave used in this experiment is called a spoof plasmon [32]. Since their discovery, the theory of spoof plasmons has been developing rapidly [48]; many structures have been proposed [33,34,36,49], including recent applications in sensors [50].

The amplification of the emission rate of selected transitions has been demonstrated by Purcell [51] in a system consisting of a Rydberg atom in a resonant cavity [52]. Here, we take advantage of this phenomenon in a very similar context for REs. The amplification of the emission rate is described by a Purcell factor [53]:

$$F = \frac{3Q}{4\pi^2 V}\left(\frac{\lambda}{n}\right)^3, \tag{3}$$

where Q is the quality factor, V is the effective mode volume (for a cavity, it is the cavity volume), and λ/n is the wavelength in the medium with refraction index n. In the case of a plasmonic structure, the mode volume can be defined as [54]

$$V = \int \frac{\rho}{\max(\rho)} d^3 r, \tag{4}$$

where ρ is the EM energy density given by [55,56]

$$\rho = \left(\epsilon + \omega\frac{\partial \epsilon}{\partial \omega}\right)|E|^2. \tag{5}$$

The second term in parentheses ensures that the energy density is positive in media with negative ϵ. The effective volume V is equal to the geometrical volume taken by the field in the case of constant field and smaller-than-geometrical volume when the field is strongly localized (like in the case of plasmons [57]). In contrast with the case of a cavity, the integration volume in Eq. (4) is not strictly defined, but only the space, where ρ (and thus the electric field) is significant, can be considered. The quality factor of the plasmonic structure is defined as

$$Q = 2\pi \frac{E}{\Delta E}, \tag{6}$$

where E is the total EM field energy contained in the system, and ΔE is energy lost in a single period of the field oscillation.

It should be mentioned that the above definition of an effective volume V is only a rough approximation [2,54], and several other approaches can be used to calculate the Purcell factor of a plasmonic system [58,59]. A detailed calculation of emission enhancement would demand a more sophisticated definition of an effective volume and inclusion of some secondary factors such as surface roughness and energy shift of excitonic levels in the vicinity of the metal-dielectric interface.

Let us consider a corrugated metal surface with multiple grooves with the depth h, width a, and period d (Fig. 1). In this paper, we consider periods d matched to the emission wavelength $\lambda \in (0.1\text{–}10)$ mm and $a, d \sim \lambda/10$. The metal

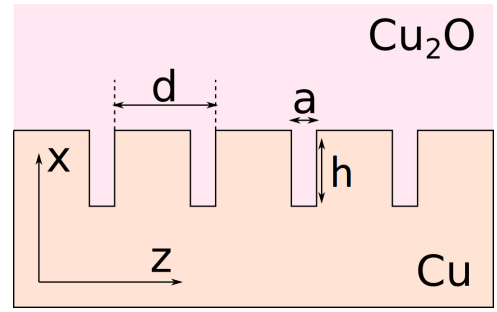

FIG. 1. Schematic representation of the system.

(Cu) is characterized by permittivity ϵ_m, and the medium inside the grooves (ϵ_g) and above them (ϵ_d) are both Cu_2O. In the considered frequency range $\omega \sim 0.3$ THz, one can assume $\epsilon_g = \epsilon_d \approx 7.5$, although it can vary depending on sample quality and temperature [60]. For metal, in this frequency range, one has $\epsilon_m = -6218 + 90i$ [61]. Note that the extremely large negative permittivity of copper means that it is a good approximation of a perfect conductor, reflecting almost 100% of incoming radiation. The effective plasma frequency of the system depicted in Fig. 1 is described by the formula $\omega_{p,\text{eff}} = \frac{\pi c}{2h\sqrt{\epsilon_g}}$ [34], and thus, in contrast with Eq. (2), it becomes dependent on the system geometry (distance h). This allows one to reduce the plasma frequency to the terahertz range.

The dispersion relation, which is derived in Ref. [48], has the form:

$$k = \left[\epsilon_d k_0^2 + \left(\frac{a\epsilon_d}{d\epsilon_g}\right)^2 k_g^2 \tan^2(k_g h)\right]^{0.5}, \tag{7}$$

where $k_0 = 2\pi f/c$ is the vacuum wave vector, and

$$k_g = k_0\sqrt{\epsilon_g}\left[1 + \frac{l_s(i+1)}{a}\right], \tag{8}$$

where $l_s = k_0 \text{Re}(\sqrt{-\epsilon_m})$ is the skin depth on the order of 30–120 nm in the terahertz range [48]. As mentioned above, in the microwave frequency range, copper can be treated as a perfect conductor. In such a case, it is possible to analytically calculate the field above the corrugated surface, provided that the grooves are considerably narrower than the wavelength [33].

First, we define the effective SPP refraction index as

$$n_{\text{eff}} = \frac{k_z}{k_0}, \tag{9}$$

where

$$\sqrt{n_{\text{eff}}^2 - 1} = \frac{a}{d}\tan(k_0 h). \tag{10}$$

Notably, the effective index and thus the optical properties are dependent only on geometric parameters of the structure (a, d, h). Thus, we have

$$k_z = k_0\sqrt{1 + \frac{a}{d}\tan(k_0 h)}, \tag{11}$$

and

$$k_x = \sqrt{k_z^2 - k_0^2}. \tag{12}$$

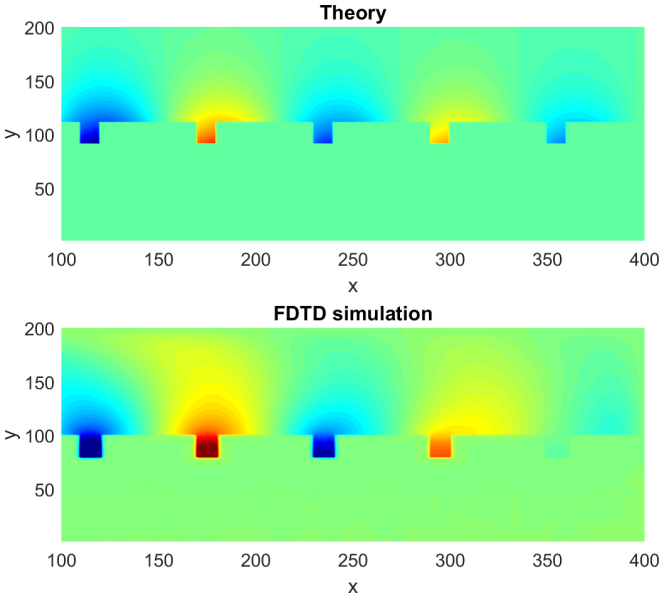

FIG. 2. Normalized field amplitude (color) obtained from Eq. (13) and finite-difference time-domain (FDTD) simulation, calculated for a structure characterized by $h = 120\,\mu\text{m}$, $a = 80\,\mu\text{m}$, and $d = 500\,\mu\text{m}$.

With the above values of wave vector components, one can use Maxwell's equations to derive the expressions describing the EM field of the spoof plasmon, which have the following forms [33]:

$$\begin{aligned} H_y &= H_0 \exp(-k_x x) \exp[i(k_z z - \omega t)], \\ E_x &= \frac{n_{\text{eff}}}{\epsilon_0 c} H_y, \\ E_z &= \frac{\sqrt{n_{\text{eff}}^2 - 1}}{i\epsilon_0 c} H_y, \end{aligned} \tag{13}$$

where H_0 is a constant dependent on the source amplitude. Having the formula for the fields, we can use Eq. (5) to calculate the energy density and then the effective volume [Eq. (4)] and Purcell factor given by Eq. (3).

It should be stressed that the direct effect of excitons on the optical properties of Cu_2O is negligible; the change of permittivity due to excitonic resonance is on the order of $\Delta\epsilon \sim 10^{-3}$, which is very small when compared with $\epsilon_b = 7.5$ [22]. Therefore, the excitonic contribution can be ignored in the calculation of the electric field distribution. The role of excitons is to provide suitable energy levels to realize microwave transition that is enhanced by the Purcell factor of the cavity.

III. FIELD AMPLIFICATION WITH SPOOF PLASMONS

Figure 2 shows a comparison between the field distribution obtained analytically from Eq. (13) and in finite-difference time-domain (FDTD) simulation, the details of which are described in Appendix A. The system is characterized by groove depth $h = 120\,\mu\text{m}$, width $a = 80\,\mu\text{m}$, and period $d = 500\,\mu\text{m}$. The operating wavelength is $\lambda \approx 1$ mm. It should be noted that Eq. (13) describes only the field above the grooved surface [33], assuming that the corrugated metal layer below is a continuous, effective medium. For this reason, while the field in Fig. 2(a) can be extended to the region inside the grooves, its values are not very accurate here. In fact, one can see that the field amplitude is somewhat greater in Fig. 2(b). However, the good match between the field distributions at the top indicates that the numerical results are accurate. The obtained results are also consistent with similar simulations performed by others authors [33–35]. One can also note that, in the theoretical distribution of the field, the metal is a perfect conductor, with no field inside. On the other hand, in FDTD simulation, the field enters the metal to a finite skin depth. Due to the limited spatial resolution $\Delta x = 10\,\mu\text{m}$, one cannot accurately measure that depth, as it is smaller than a single unit cell.

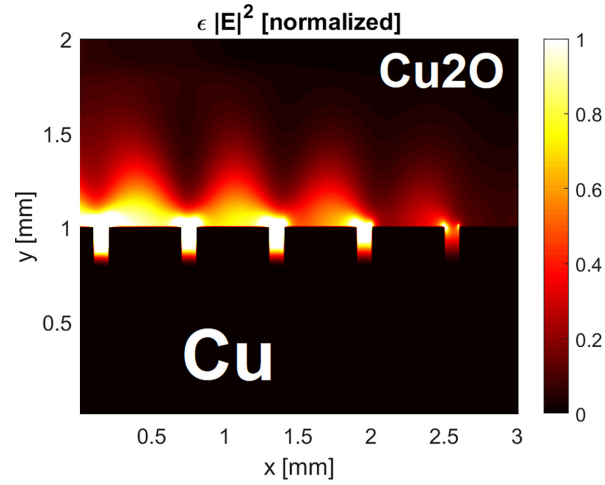

FIG. 3. Normalized energy density of the corrugated surface structure illuminated by $\lambda = 1$ mm light; the same geometry as in Fig. 2.

The important property of the system is the fact that the field is focused into deep subwavelength regions inside the grooves. Figure 3 shows the time-averaged normalized field energy density in the system obtained in FDTD simulation. The concentration of energy in subwavelength spots greatly reduces the effective mode volume given by Eq. (4); for the discussed system, one obtains $V \approx 0.018 V_g$, where $V_g = \lambda^3$ is the geometric volume of the cavity. This result is comparable with the $V = 0.015 V_g$ reported in Ref. [62] for a metal-dielectric-metal system. For further comparison, an effective volume of $0.01 V_g$ is obtained in plasmonic particles [54] and up to 10^{-6} in a bow-tie antenna [63]. Overall, the grooved surface (also known as a nanoslit cavity) offers very small mode volume and relatively high Q factor as compared with other plasmonic structures [64].

The Q factor is strongly dependent on the geometry details; usually, it is on the order of 10^2 [50,62], but with the introduction of defects in the form of single shorter/longer grooves, it can reach 10^5 [34]. Moreover, at microwave frequencies, it is relatively straightforward to introduce gain to the system, increasing the Q factor to 10^5 [65]. For the simulated structure shown in Fig. 2, the Q factor has been estimated at $Q = 124$. While the Q factor is considerably lower than in

regular cavities, the low mode volume still allows for a large Purcell factor [53].

With this in mind, we can calculate the Purcell factor from Eq. (3), obtaining $F \sim 530$. Again, the result is consistent with Purcell factors obtained in the visible spectrum of plasmonic structures; in Ref. [54], $F \sim 10^2$–10^5 is reported in nanospheres depending on sphere diameter. The value of $F \approx 2000$ is demonstrated for Ag nanocubes [66]. Maier [62] reported $F \sim 3400$ for the optical spectrum, mentioning that, for far infrared wavelengths, values exceeding 10^4 are possible. For metamaterial-dielectric interfaces, similar conclusions are reported [67]. For the microwave frequency range, an analysis of the Purcell factor of a thin-wire-type plasmonic material yields $F \sim 10^2$–10^3 and up to 10^6 for radio frequencies [59].

To investigate the potential of the corrugated metallic surface to improve the probability of microwave transitions, one first needs to optimize its geometry. Again, we consider the structure from Fig. 1 and perform FDTD simulations to obtain the EM field distribution. The simulations are two-dimensional, which implies that the system is large (longer than wavelength) in the y axis. However, as noted in Ref. [36], the properties of spoof plasmons on such a structure depend very weakly on the thickness in the y axis, so that the results are applicable even to 10-nm-thin films. This will be an important point later when Rydberg blockade is discussed. Moreover, we set the structure period fixed at $d = 1$ mm, which is equal to the operating wavelength. In simulations, this value provided the best results regardless of other system dimensions; the match to the wavelength facilitates the formation of strong standing-wave-type plasmons with high field intensity. The Purcell factor F and the structure Q factor as a function of the groove depth h and width a are shown in Fig. 4. One can see in Fig. 4(a) that the system has several distinct regimes of operation; in the limit of a very narrow groove, the field inside is highly focused, resulting in a small effective volume and considerable Purcell factor. Then a second local maximum occurs at $a \approx 0.2$ λ. As will be shown later, depending on the groove height h, this maximum is located at 0.2–0.3 λ and in general corresponds to the system where the groove acts as a quarter-wave cavity. Finally, a third, small maximum can be seen at $a \approx 0.5$ λ, which again facilitates the formation of standing waves.

The quality factor of the structure is approximately $Q \sim 100$ and shows relatively little variation with a, with the exception of a very narrow grooves. However, from the simulation results, it is inconclusive if the increase of Q is the feature of a narrow-gap SPP or the result of weaker coupling of the free space field to the plasmons; the stray waves that freely propagate through Cu_2O above the corrugated surface are very weakly attenuated, and as such, they spuriously increase the estimated Q factor calculated from the propagation length. We stress that the value Q serves only as a general estimation and is affected by many factors such as surface roughness that are omitted here.

The dependence of F on the groove height shown in Fig. 4(b) exhibits one large local maximum at $h = 0.25$ λ. As noticed in Ref. [48], this is the expected result; the most efficient focusing of the field occurs when the grooves act as quarter-wave antennas. Interestingly, the Q factor exhibits a

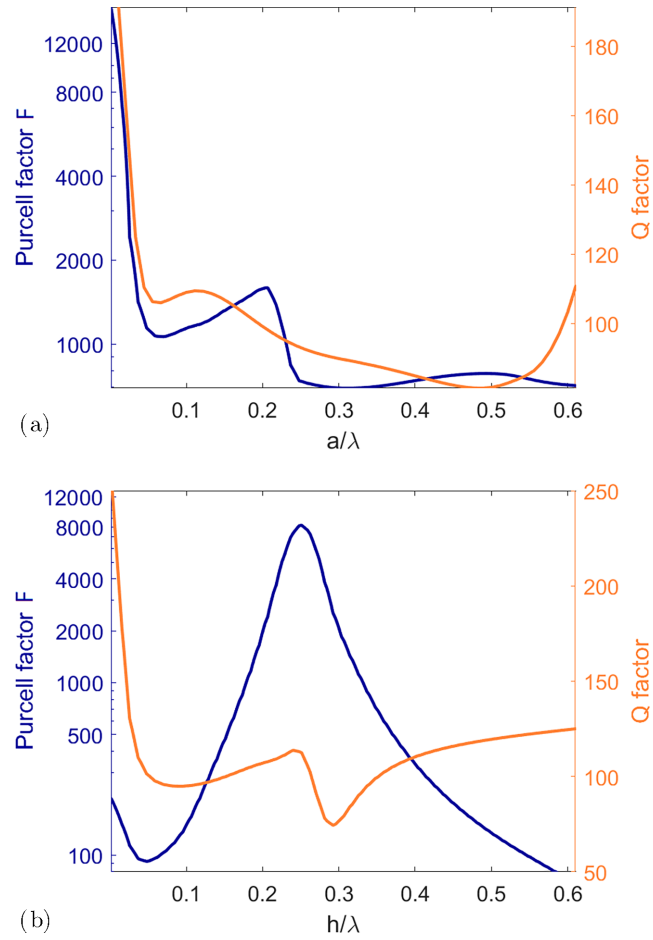

FIG. 4. Purcell factor F and Q factor of the structure as a function of (a) width a and (b) depth h. Structure is illuminated by $\lambda = 1$ mm light.

local drop at this point. As noted in Ref. [35], well-defined SPPs are only possible when $h > d/2$. In our case, when $d = \lambda/2$, the limit is $h > \lambda/4$, which is exactly the point where the drop in the Q factor occurs. This means that, as h increases, the system transitions from a mix of surface plasmons and free propagating waves to one where the energy is located mostly in surface plasmons. As a result, the propagation distance is shortened, and the Q factor is reduced.

The optimization performed over the full parameter space of a and h is shown in Fig. 5. The main feature of the figure is a wide maximum that corresponds to $h = 0.25$ λ for most values of a and approaches $h = 0.2$ λ for $a \to 0$. As mentioned above, in general, the Purcell factor reaches the maximum value for $h = 0.25$ λ. However, for very narrow grooves, the maximum shifts toward $h = 0.2$ λ due to the fact that the wave vector k_z given by the dispersion relation given in Eq. (11) differs considerably from the free space wave vector k_{z0} in the limit if $a \to 0$. In such a case, the wavelength is no longer equal to the nominal value of 1 mm, and so the system is detuned from the chosen microwave transition.

The system geometry determines the upper limit of the emission power. For example, with $\lambda = 1$ mm, $h = 0.25\lambda$, and $a = 0.2\lambda$, the total geometrical volume of the cavity is $V_g = 5 \times 10^7\ \mu m^3$. Assuming that we use, for example,

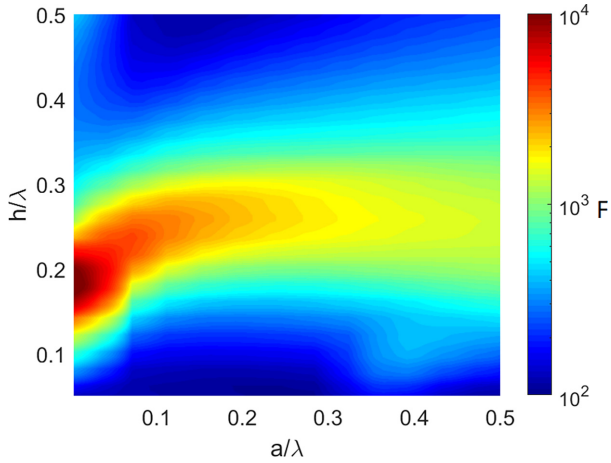

FIG. 5. Purcell factor F of the structure as a function of a and h, $\lambda = 1$ mm.

$n = 10$ excitonic level, from Eq. (1), one has $V_b = 3\,\mu\text{m}^3$, and thus, the number of excitons in the cavity is $N \sim 3 \times 10^6$. This number, in conjunction with the Purcell effect-boosted emission rate, allows one to estimate the number of emitted photons.

IV. ENHANCED MICROWAVE EMISSION

With the results presented in the last section, we can conclude that the Purcell factor $F \sim 10^5$ is possible in the discussed system. Now we can investigate how such an enhancement affects the exciton population dynamics in Cu_2O. To perform such a consideration, let us assume that the system is illuminated by a light beam with frequency matched to the energy of an $n = 8$ exciton (2170.6 meV, 571 nm). The light intensity is sufficient to saturate the system, i.e., create the exciton density that approaches the limit imposed by Rydberg blockade; a single $n = 8$ exciton is characterized by a blockade volume $V_B \approx 0.63\,\mu\text{m}^3$, and so the upper limit of the exciton density is $N_{\max} \approx 1.6 \times 10^{12}$ cm^{-3}. The wavelength for transition $n = 8 \to n = 6$ of $\lambda_{86} \approx 1.06$ mm is a close match to the idealized 1-mm wavelength discussed earlier. The point of interest is the transition rate γ_{86} and how it compares with the most probable transition of the $n = 8$ exciton back to the ground state, described by $\gamma_8 \approx 12.3$ GHz, $\hbar\gamma_8 \approx 25\,\mu\text{eV}$ [13,21]. The rates are calculated on the basis of the overlap of hydrogenlike wave functions of $n = 8$ and 6 states, as described in Refs. [11,21] and in Appendix A. Here, they result in $\gamma_{86} \approx 9.8$ kHz. The lower-state relaxation rate is $\gamma_6 \approx 24.2$ GHz, $\hbar\gamma_8 \approx 36.7\,\mu\text{eV}$. The results for a system with $h = 0.25\ \lambda$ are shown in Fig. 6(a). As expected, in the limit of a narrow groove, the large Purcell factor results in the highest transition rate γ_{86}. In this regime, the fraction γ_{86}/γ_8 approaches 1% which means that, on average, for every 100 decaying $n = 8$ excitons, one of them will return to the ground state through the intermediate state $n = 6$, emitting a microwave photon in the process. However, the emission power is proportional to the number of created excitons $N \sim \frac{V_g}{V_b}$, and thus, it is relatively small in the case of a very narrow cavity with small volume V_g. Like in the earlier result

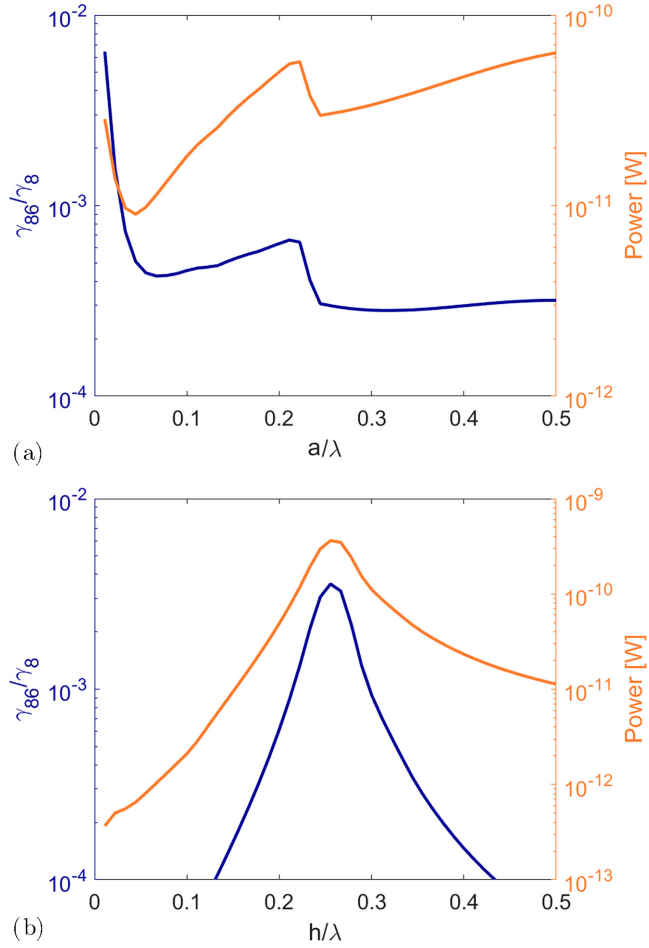

FIG. 6. The ratio of the transition rates γ_{86}/γ_8 and the microwave emission power as a function of (a) a and (b) h; $\lambda = 1$ mm.

in Fig. 4, the optimal operating point for power is the local maximum of the Purcell factor at $a \sim 0.2\ \lambda$ [Fig. 6(a)]. A similar optimization can be performed for the parameter h. In this case, $h = \lambda/4$ is a global maximum for both power and transition rate [Fig. 6(b)]. This general characteristic is maintained in systems with different combinations of excitonic states. A full overview is presented in Fig. 7. The calculations have been performed for pairs of all states $[n_1, n_2]$, $n_1 > n_2$ up to $n_1 = 25$. The emission power is given by

$$P = N\hbar\omega_{n_1,n_2}\gamma_{n_1,n_2}F, \tag{14}$$

where N is the average number of excitons inside the groove. The aim is to illustrate some general tendencies and orders of magnitude, and thus, the quality factor is set to $Q = 100$, and the Purcell factor is assumed to be $F = 10^4$. The plasmonic system is characterized by $a = 0.2\ \lambda_{n_1,n_2}$ and $h = 0.25\lambda_{n_1,n_2}$. A more thorough analysis of any particular state combination would warrant full geometry optimization for the given transition wavelength λ_{n_1,n_2}. The illuminating optical beam is assumed to be strong enough to saturate the system with excitons up to the limit imposed by Rydberg blockade. One can notice that the emission wavelength in Fig. 7 is the most dependent on the choice of the lower excitonic level, with much smaller contribution from the upper level. This is a direct consequence of the energy spacing of excitonic levels

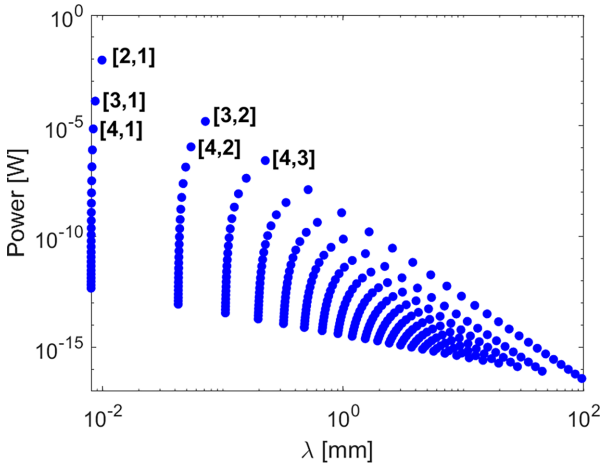

FIG. 7. The maximum microwave emission power as a function of wavelength; excitonic state combinations $[n_1, n_2]$; in each system, $a = 0.2\lambda$, $h = 0.25\lambda$, and $d = 0.5\lambda$.

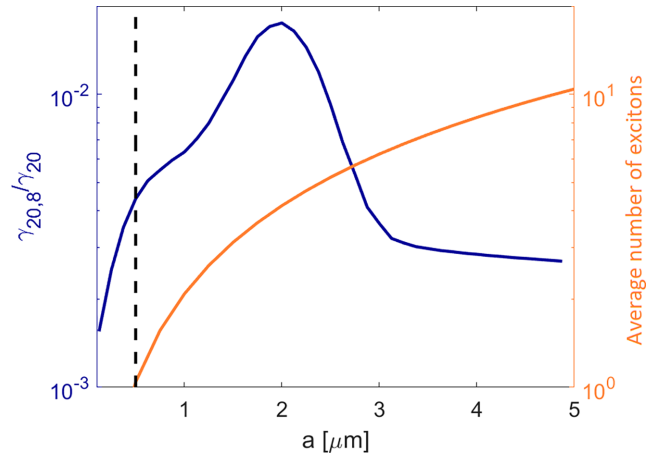

FIG. 8. The ratio of the transition rates $\gamma_{20,8}/\gamma_{20}$ and the number of excitons inside a single groove as a function of a.

$\delta E \sim n^{-1}$. The power decreases very quickly with n due to several factors; the number of excitons in the system is inversely proportional to blockade volume of the excitons created by the optical field, which scales as n_1^7. Moreover, the longer wavelength photons have smaller energy, which introduces another scaling factor $\sim\lambda_{n_1 n_2}^{-1}$. The peak power is 10^{-2} W; however, it should be noted that the conversion efficiency is on the order of 10^{-2}, and the ratio of optical photon to microwave photon energy is $\sim 10^3$; so overall, the maximum predicted power output would demand $P \sim 10^3$ W of optical power, which could only be feasibly realized in pulsed operation. In general, the obtained power and efficiency figures are superior to approaches using nonlinear processes and comparable with the recently proposed plasmon-coupled surface state device [68]. The highest obtained power corresponds to the photon emission rate in excess of 10^{16} per second.

One interesting possibility is to take advantage of the large blockade volume of excitons characterized by large principal quantum number n to facilitate single photon emission. Khazali *et al.* [69] proposed a system where only a single exciton could fit inside a Cu_2O nanocrystal, which resulted in the emission of a single photon when it decayed. Here, we propose a microwave analog of this system by using extremely narrow grooves. Specifically, let us consider a system characterized by $h = \lambda/4$ and $a < 5\,\mu$m. The thickness of the system on the y axis is $b = 10\,\mu$m. The excited state is $n = 20$, and the system is matched to the transition $n = 20 \rightarrow n = 8$, which is characterized by a wavelength $\lambda \approx 0.98$ mm. The results are shown in Fig. 8. Due to the large dipole moment of the $n = 20 \rightarrow n = 8$ transition and longer lifetime of the $n = 20$ exciton, the ratio $\gamma_{20,8}/\gamma_{20}$ is slightly larger than in the last system, reaching peak efficiency of 1.7% for $a = 2\,\mu$m. As mentioned in Ref. [48], the capability of the system to focus the EM field is limited by the skin depth of the metal, which in the terahertz range is on the order of 120 nm. One can see that, in this particular example, the transition rate sharply decreases when $a < 500$ nm (dashed line), which is four times the skin depth. At the point of peak efficiency, the average number of excitons that fit inside the groove is on the order of 10. It should be mentioned that, since the exciton size is comparable with the groove width a, a more thorough analysis involving confined excitonic states [16,17] and their interaction with metallic surfaces [70] would be needed to fully describe the system. Nevertheless, it is clear that, with sufficient reduction of the groove width, one can easily fabricate a system where a single exciton serves as a source of single microwave photons.

V. CONCLUSIONS

We have proposed a copper-based plasmonic system that facilitates microwave-to-optical frequency conversion with the use of excitonic states in Cu_2O. The described scheme takes advantage of the capability of surface plasmons to amplify and focus the field in subwavelength areas, which facilitates the enhancement of transition probabilities with the Purcell effect. We focus on the microwave frequency transitions between highly excited levels of REs in Cu_2O. It is shown that, with proper geometry, one can use the so-called spoof plasmons to reduce the plasmon frequency to the microwave range, allowing for efficient plasmon-RE coupling. With optimal geometry, the amplification of the probability of specific microwave transitions is on the order of 10^3, with values up to 10^5 being feasible. This, in turn, provides relatively large conversion efficiency of $>1\%$ [2]. Finally, the possibility of single-photon emission with the use of Rydberg blockade is investigated. The system geometry (corrugated surface) and materials (copper and copper oxide) are characterized by low cost and ease of fabrication, and due to the large number of available excitonic levels, one can choose transitions within a large range of wavelengths (0.1–10 mm) [21].

ACKNOWLEDGMENT

Support from the National Science Centre, Poland (NCN), project Miniatura, 2022/06/X/ST3/01162, is acknowledged.

APPENDIX A: FDTD METHOD

For numerical calculations of the field distribution around the plasmonic structure, we use the FDTD method [71], which

is based directly on Maxwell's equations and provides high flexibility and accuracy in modeling the propagation of EM waves. To reduce computational demands, we assume that the system is two-dimensional, e.g., the system depicted in Fig. 1 is much larger than the wavelength on the y axis. The computation domain is divided by a rectangular grid with a single cell size $\Delta x = 10\,\mu$m, and the EM field components corresponding to waves propagating on the xz plane ($\vec{E} = [E_x, 0, E_z]$ and $\vec{H} = [0, H_y, 0]$) are calculated with evolution formulas derived from Maxwell's equations. Specifically,

$$\frac{\partial H_y}{\partial t} = \frac{1}{\mu_0}\left(\frac{\partial E_x}{\partial z} - \frac{\partial E_z}{\partial x}\right), \tag{A1}$$

$$\frac{\partial E_x}{\partial t} = \frac{1}{\epsilon_0}\left(\frac{\partial H_y}{\partial z} - \frac{\partial P_x}{\partial t} + j_x\right), \tag{A2}$$

$$\frac{\partial E_z}{\partial t} = \frac{1}{\epsilon_0}\left(\frac{\partial E_x}{\partial z} - \frac{\partial P_z}{\partial t} + j_z\right), \tag{A3}$$

where j_x,j_z are components of current density, ϵ_0, μ_0 are the vacuum permittivity and permeability, respectively, and P is medium polarization. The above equations are discretized with a fixed time step Δt and rearranged to obtain time derivatives of the E_x, E_z, and H_y fields, which are used to calculate next field values from current ones iteratively. In the calculations, a unit normalization is used so that $\epsilon_0 = \mu_0 = c = 1$, $\Delta_x = 1$, and $\Delta t = 0.5$. The time and spatial step satisfy the Courant stability criterion [72]:

$$\frac{c\Delta t}{\Delta x} < \frac{1}{\sqrt{2}}. \tag{A4}$$

For the considered system, the wavelength $\lambda = 1$ mm is equal to 100 spatial steps, and thus, the numerical frequency is

$$\omega = \frac{2\pi c}{\lambda} \approx 0.063. \tag{A5}$$

The dispersive properties of media are included with the use of an auxiliary differential equation (ADE) approach [73], where the time evolution of polarization vector $\vec{P} = [P_x, 0, P_z]$ is described by a second-order partial differential equation:

$$\ddot{\vec{P}} + \Gamma_j \dot{\vec{P}} + \omega_j = \frac{\epsilon_0 f_j}{\epsilon_\infty}\vec{E}, \tag{A6}$$

with a constant permittivity ϵ_∞ and a set of fitted oscillator terms $j = 1, 2, 3\ldots$ characterized by oscillator strength f_j, damping Γ_j, and resonant frequency ω_j. For the example of the system considered here, the surface plasmon is generated by a monochromatic wave, and thus, it has a relatively narrow spectrum. In such a case, the dispersion of copper oxide is negligible, and thus, it can be characterized by a constant $\epsilon_\infty = 7.5$. For copper, we use the Drude model described by Eq. (A6), with a single oscillatory term characterized by $f_1 = 24.6875$, $\Gamma_1 = 0.000916$, and $\omega_1 = 0$. In the frequency domain, the copper permittivity is given by

$$\epsilon(\omega) = 1 - \frac{f_1}{\omega^2 + i\Gamma_1\omega}. \tag{A7}$$

For the above-mentioned frequency $\omega = 0.063$, one obtains $\epsilon(\omega) = -6218 + 90i$, which is consistent with Ref. [61].

The calculation is performed for a system depicted in Fig. 2, with numerical grid size of 400×200 points (4 and 2 mm, respectively). A line source of radiation (a single point on the xz plane) is used to excite surface plasmons. After steady plasmon field amplitude is reached, the source is turned off. Then the energy density is calculated according to Eq. (5). The decay of total field energy in time is used to estimate the Q factor of the system.

APPENDIX B: EXCITONIC INTERLEVEL TRANSITION RATES

To calculate the probability of transition between two selected excitonic levels $n_2 \to n_1$, we recall that the change of the density of excitons η_2 is given by

$$\frac{\partial \eta_2}{\partial t} = -\gamma_{21}\eta_2 = -(A_{21} + B_{21}\rho)\eta_2, \tag{B1}$$

where γ_{21} is the interlevel transition rate, ρ is EM field density [Eq. (5)], A_{21} is the Einstein coefficient of spontaneous emission, and B_{21} is the coefficient of stimulated emission. They are given by [74]

$$\begin{aligned} A_{21} &= \frac{2\omega_{21}^3}{3\epsilon_0\hbar c^3}|d_{21}|^2 F, \\ B_{21} &= \frac{\pi}{3\epsilon_0\hbar^2}|d_{21}|^2 F, \end{aligned} \tag{B2}$$

where d_{21} is the transition dipole operator, and F is the Purcell factor. The REs are characterized by a hydrogenlike wave function:

$$\psi(r, \theta, \phi) = R(r)Y_{lm}(\theta, \phi), \tag{B3}$$

where Y_{lm} are spherical harmonics, and $R(r)$ is the radial part. The dipole moment is given by

$$d_{21} = \langle\psi_f|er|\psi_i\rangle = \int \psi_f^* er \psi_i d^3 r. \tag{B4}$$

For the radiative transitions $n_2P \to n_1S$, $\Delta l = 1$, and $m = 0$, the angular part of the above expression is a constant [75]:

$$\int Y^*_{l_f m_f} Y_{l_i m_i} \sin\theta d\theta d\phi = \frac{1}{\sqrt{3}}, \tag{B5}$$

and the radial part:

$$R_{if} = 4\pi \int R^*_{n_f,l_f}(r) R_{n_i,l_i}(r) r^3 dr, \tag{B6}$$

can be calculated numerically. In general, it is strongly dependent on the principal quantum number [11]. For the exciton transition to the ground state, we can use established, experimentally measured values [13], which can be described by an expression:

$$\gamma_n = 24\,\text{meV}\,\frac{1 + 0.01n^2}{n^3}, \tag{B7}$$

while interlevel transition rates γ_{12} are given by Eq. (B1). In summary, to calculate the emission rate, one needs to calculate the above-mentioned dipole moment, the Purcell coefficient as outlined in Eq. (3), and estimate the exciton density η_2. As a

first step, one can assume that the system is saturated up to the level allowed by Rydberg blockade and thus use

$$\eta_2 = \frac{1}{V_b}, \tag{B8}$$

where $V_b = 3 \times 10^{-7}\,\mu\text{m}^3 \cdot n^7$ is the blockade volume [13] of the exciton with principal quantum number n. It should be stressed that this value represents an upper limit; in practice, some of the volume will be taken by excitons n_1 and other excitonic states involved in various transitions that are partially tuned to the plasmonic structure. However, since n_2 is the highest state in the system and the blockade volume scales as n^7, the contribution of these lower states is limited. Finally, to estimate the input power, one can use

$$P_{in} = E_2 \eta_2 \tau_2 V, \tag{B9}$$

where E_2 is the energy of a single exciton, $\tau_2 = 1/(\Gamma_2 + \gamma_{21})$ is its lifetime, and V is the emission volume (in our case, a single groove/cavity). Therefore, the output power and conversion efficiency (ratio of output to input power) are highly complex functions of exciton lifetime, energy, dipole density of specific transition, and Purcell factor of the cavity.

[1] X. Han, W. Fu, C. Zou, L. Jiang, and H. X. Tang, Microwave-optical quantum frequency conversion, Optica **8**, 1050 (2021).

[2] N. J. Lambert, A. Rueda, F. Sedlmeir, and H. G. L. Schwefel, Coherent conversion between microwave and optical photons—An overview of physical implementations, Adv. Quantum Technol. **3**, 1900077 (2020).

[3] T. Zhong and P. Goldner, Emerging rare-earth doped material platforms for quantum nanophotonics, Nanophotonics **8**, 2003 (2019).

[4] G. Wendin, Quantum information processing with superconducting circuits: A review, Rep. Prog. Phys. **80**, 106001 (2017).

[5] Y. T. Chau, H. Huang, M. Nguyen, K. Hatanaka, and T. Yonezawa, THz wave emission from the Cu_2O/Cu interface under femtosecond laser irradiation, Appl. Phys. Express **14**, 012006 (2021).

[6] G. K. P. Ramanandan, A. J. L. Adam, G. Ramakrishnan, P. Petrik, R. Hendrikx, and P. C. M. Planken, Optical characterization of gold-cuprous oxide interfaces for terahertz emission applications, Appl. Opt. **53**, 1994 (2014).

[7] A. Gupta, G. Rana, A. Bhattacharya, A. Singh, R. Jain, R. D. Bapat, S. P. Duttagupta, and S. S. Prabhu, Enhanced optical-to-THz conversion efficiency of photoconductive antenna using dielectric nano-layer encapsulation, APL Photonics **3**, 051706 (2018).

[8] I. V. Oladyshkin, D. A. Fadeev, and V. A. Mironov, Optical excitation of surface plasmons and terahertz emission from metals, Phys. Rev. B **100**, 085421 (2019).

[9] D. H. Auston, K. P. Cheung, and P. R. Smith, Picosecond photoconducting Hertzian dipoles, Appl. Phys. Lett. **45**, 284 (1984).

[10] C. Wang, Z. Zhang, Y. Zhang, X. Xie, Y. Yang, J. Han, E. Li, H. Chen, J. Gu, W. E. I. Sha *et al.*, Enhancing directivity of terahertz photoconductive antennas using spoof surface plasmon structure, New J. Phys. **24**, 073046 (2022).

[11] D. Ziemkiewicz and S. Zielińska-Raczyńska, Solid-state pulsed microwave emitter based on Rydberg excitons, Opt. Express **27**, 16983 (2019).

[12] B. T. Gard, K. Jacobs, R. McDermott, and M. Saffman, Microwave-to-optical frequency conversion using a cesium atom coupled to a superconducting resonator, Phys. Rev. A **96**, 013833 (2017).

[13] T. Kazimierczuk, D. Fröhlich, S. Scheel, H. Stolz, and M. Bayer, Giant Rydberg excitons in the copper oxide Cu_2O, Nature (London) **514**, 343 (2014).

[14] A. Poddubny and M. Glazov, Topological Spin Phases of Trapped Rydberg Excitons in Cu_2O, Phys. Rev. Lett. **123**, 126801 (2019).

[15] D. Ziemkiewicz, G. Czajkowski, K. Karpiński, and S. Zielińska-Raczyńska, Rydberg magnetoexcitons in Cu_2O quantum wells, Phys. Rev. B **103**, 035305 (2021).

[16] K. Orfanakis, S. Rajendran, H. Ohadi, S. Zielińska-Raczyńska, G. Czajkowski, K. Karpiński, and D. Ziemkiewicz, Quantum confined Rydberg excitons in Cu_2O nanoparticles, Phys. Rev. B **103**, 245426 (2021).

[17] A. Konzelmann, B. Frank, and H. Giessen, Quantum confined Rydberg excitons in reduced dimensions, J. Phys. B: At. Mol. Opt. Phys. **53**, 024001 (2020).

[18] S. Steinhauer, M. Versteegh, S. Gyger, A. Elshaari, B. Kunert, A. Mysyrowicz, and V. Zwiller, Rydberg excitons in Cu2O microcrystals grown on a silicon platform, Commun. Mater. **1**, 2 (2020).

[19] M. Takahata, K. Tanaka, and N. Naka, Nonlocal optical response of weakly confined excitons in Cu_2O mesoscopic films, Phys. Rev. B **97**, 205305 (2018).

[20] R. Huber, B. A. Schmid, Y. R. Shen, D. S. Chemla, and R. A. Kaindl, Stimulated Terahertz Emission from Intraexcitonic Transitions in Cu_2O, Phys. Rev. Lett. **96**, 017402 (2006).

[21] D. Ziemkiewicz and S. Zielińska-Raczyńska, Proposal of tunable Rydberg exciton maser, Opt. Lett. **43**, 3745 (2018).

[22] D. Ziemkiewicz and S. Zielińska-Raczyńska, Copper plasmonics with excitons, Phys. Rev. B **106**, 205404 (2022).

[23] J. Khurgin, Pliable polaritons: Wannier exciton-plasmon coupling in metal-semiconductor structures, Nanophotonics **8**, 629 (2019).

[24] N. Weber, S. P. Hoffmann, M. Albert, T. Zentgraf, and C. Meier, Efficient frequency conversion by combined photonic-plasmonic mode coupling, J. Appl. Phys. **123**, 103101 (2018).

[25] Q. Shen, A. Shams-Ansari, A. M. Boyce, N. C. Wilson, T. Cai, M. Loncar, and M. H. Mikkelsen, A metasurface-based diamond frequency converter using plasmonic nanogap resonators, Nanophotonics **10**, 589 (2021).

[26] A. Agreda, D. Sharma, G. Francs, G. Kumar, and A. Bouhelier, Modal and wavelength conversions in plasmonic nanowires, Opt. Express **29**, 15366 (2021).

[27] N. Fofang, T. Park, O. Neumann, N. Mirin, P. Nordlander, and N. Halas, Plexcitonic nanoparticles: Plasmon-exciton coupling in nanoshell-J-aggregate complexes, Nano Lett. **8**, 3481 (2008).

[28] E. Karademir, S. Balci, C. Kocabas, and A. Aydinli, Plexcitonic crystals: A tunable platform for light-matter interactions, Opt. Express **22**, 21912 (2014).

[29] H. Lee, D. Luong, M. Kim, Y. Jin, H. Kim, S. Yun, and Y. Lee, Reconfigurable exciton-plasmon interconversion for nanophotonic circuits, Nat. Commun. **7**, 13663 (2016).

[30] E. Cao, W Lin, M. Sun, W. Liang, and Y. Song, Exciton-plasmon coupling interactions: From principle to applications, Nanophotonics **7**, 145 (2018).
[31] P. A. D. Gonçalves, L. Bertelsen, S. Xiao, and N. Mortensen, Plasmon-exciton polaritons in two-dimensional semiconductor/metal interfaces, Phys. Rev. B **97**, 041402(R) (2018).
[32] J. B. Pendry, L. Martin-Moreno, and F. J. Garcia-Vidal, Mimicking surface plasmons with structured surfaces, Science **305**, 847 (2004).
[33] L. Kong, C. Huang, C. Du, P. Liu, and X. Yin, Enhancing spoof surface-plasmons with gradient metasurfaces, Sci. Rep. **5**, 8772 (2015).
[34] S. R. Joy, M. Erementchouk, and P. Mazumde, Spoof surface plasmon resonant tunneling mode with high quality and Purcell factors, Phys. Rev. B **95**, 075435 (2017).
[35] M. Erementchouk, S. Roy Joy, and P. Mazumder, Electrodynamics of spoof plasmons in periodically corrugated waveguides, Proc. R. Soc. A **472**, 20160616 (2016).
[36] W. Tang, H. Zhang, H. Ma, W. Jiang, and T. Cui, Concept, theory, design, and applications of spoof surface plasmon polaritons at microwave frequencies, Adv. Opt. Mater. **7**, 1800421 (2019).
[37] G. Chan, J. Zhao, E. Hicks, G. Schatz, and R. Van Duyne, Plasmonic properties of copper nanoparticles fabricated by nanosphere lithography, Nano Lett. **7**, 1947 (2007).
[38] V. Mkhitaryan, K. March, E. Tseng, X. Li, L. Scarabelli, L. Liz-Marzán, S. Chen, L. Tizei, O. Stéphan, J. Song *et al.*, Can copper nanostructures sustain high-quality plasmons? Nano Lett. **21**, 2444 (2021).
[39] O. Peña-Rodríguez and U. Pal, Effects of surface oxidation on the linear optical properties of Cu nanoparticles, J. Opt. Soc. Am. B **28**, 2735 (2011).
[40] J. Sancho-Parramon, B. Okorn, K. Salamon, and V. Janicki, Plasmonic resonances in copper island films, Appl. Surf. Sci. **463**, 847 (2019).
[41] A. Böhme, F. Sterl, E. Kath, M. Ubl, V. Manninen, and H. Giessen, Electrochemistry on inverse copper nanoantennas: Active plasmonic devices with extraordinarily large resonance shift, ACS Photonics **6**, 1863 (2019).
[42] C. de Melo, M. Jullien, Y. Battie, A. Naciri, J. Ghanbaja, F. Montaigne, J. Pierson, F. Rigoni, N. Almqvist, A. Vomiero *et al.*, Tunable localized surface plasmon resonance and broadband visible photoresponse of Cu nanoparticles/ZnO surfaces, ACS Appl. Mater. Inter. **10**, 40958 (2018).
[43] C. Huang, G. Kumar, G. Sharma, and F. Chen, Plasmonic effects of copper nanoparticles in polymer photovoltaic devices for outdoor and indoor applications, Appl. Phys. Lett. **116**, 253302 (2020).
[44] X. Zhang, Q. Xu, L. Xia, Y. Li, J. Gu, Z. Tian, C. Ouyang, J. Han, and W. Zhang, Terahertz surface plasmonic waves: A review, Adv. Photonics **2**, 014001 (2020).
[45] L. A. P. Gallagher, J. P. Rogers, J. D. Pritchett, R. A. Mistry, D. Pizzey, C. S. Adams, and M. P. A. Jones, Microwave-optical coupling via Rydberg excitons in cuprous oxide, Phys. Rev. Res. **4**, 013031 (2022)
[46] J. B. Pendry, A. J. Holden, D. J. Robbins, and W. J. Stewart, Low frequency plasmons in thin-wire structures, J. Phys.: Condens. Matter **10**, 4785 (1998).
[47] R. A. Shelby, D. R. Smith, S. C. Nemat-Nasser, and S. Schultz, Microwave transmission through a two-dimensional, isotropic, left-handed metamaterial, Appl. Phys. Lett. **78**, 489 (2001).
[48] A. Rusina, M. Durach, and M. I. Stockman, Theory of spoof plasmons in real metals, Appl. Phys. A **100**, 375 (2010).
[49] X. Shen and T. Jun Cui, Ultrathin plasmonic metamaterial for spoof localized surface plasmons, Laser Photonics Rev. **8**, 137 (2014).
[50] J. Wang, J. Zhang, H. Gao, X. Fu, D. Bao, and T. Cu, Mixed-resolution high-Q sensor based on hybridized spoof localized surface plasmons, Front. Phys. **10**, 850186 (2022).
[51] E. M. Purcell, Spontaneous emission probabilities at radio frequencies, Phys. Rev. **69**, 37 (1946).
[52] Y. Todorov, I. Sagnes, I. Abram, and C. Minot, Purcell Enhancement of Spontaneous Emission from Quantum Cascades inside Mirror-Grating Metal Cavities at THz Frequencies, Phys. Rev. Lett. **99**, 223603 (2007).
[53] G. Colas des Francs, J. Barthes, A. Bouhelier, J. C. Weeber, A. Dereux, A. Cuche, and C. Girard, Plasmonic Purcell factor and coupling efficiency to surface plasmons. Implications for addressing and controlling optical nanosources, J. Opt. **18**, 094005 (2016).
[54] A. F. Koenderink, On the use of Purcell factors for plasmon antennas, Opt. Lett. **35**, 4208 (2010).
[55] L. D. Landau and E. M. Lifshitz, *Electrodynamics of Continuous Media*, 2nd ed. (Pergamon Press, Oxford, 1984).
[56] F. D. Nunes, T. C. Vasconcelos, M. Bezerra, and John Weiner, Electromagnetic energy density in dispersive and dissipative media, J. Opt. Soc. Am. B **28**, 1544 (2011).
[57] C. Feuillet-Palma, Y. Todorov, R. Steed, A. Vasanelli, G. Biasiol, L. Sorba, and C. Sirtor, Extremely sub-wavelength THz metal-dielectric wire microcavities, Opt. Express **20**, 29121 (2012).
[58] C. R. Simovski, P. A. Belov, A. V. Atrashchenko, and Y. S. Kivshar, Wire metamaterials: Physics and applications, Adv. Mater. **24**, 4229 (2012).
[59] A. N. Poddubny, P. A. Belov, and Y. S. Kivshar, Purcell effect in wire metamaterials, Phys. Rev. B **87**, 035136 (2013).
[60] F. L. Weichman, Some rationale for the unusual behavior of the dielectric constant of Cu_2O, Can. J. Phys. **51**, 680 (1973).
[61] A. S. Tukmakova, A. V. Asach, A. V. Novotelnova, L. Tkhorzhevskiy, N. S. Kablukova, P. S. Demchenko, A. D. Zaitsev, and M. K. Khodzitsky, FEM simulation of THz detector based on Sb and $Bi_{88}Sb_{12}$ thermoelectric thin films, Appl. Sci. **10**, 1929 (2020).
[62] S. A. Maier, Plasmonic field enhancement and SERS in the effective mode volume picture, Opt. Express **14**, 1957 (2006).
[63] Z. Yang, T. Antosiewicz, and T. Shegai, Role of material loss and mode volume of plasmonic nanocavities for strong plasmon-exciton interactions, Opt. Express **24**, 20373 (2016).
[64] K. Chen, G. Razinskas, H. Vieker, H. Gross, X. Wu, A. Beyer, A. Gölzhäuser, and B. Hecht, High-Q, low-mode-volume and multiresonant plasmonic nanoslit cavities fabricated by helium ion milling, Nanoscale **10**, 17148 (2018).
[65] J. Cai, Y. Jin Zhou, Y. Zhang, and Q. Yu Li, Gain-assisted ultra-high-Q spoof plasmonic resonator for the sensing of polar liquids, Opt. Express **26**, 25460 (2018).
[66] G. M. Akselrod, C. Argyropoulos, T. B. Hoang, C. Ciraci, C. Fang, J. Huang, D. R. Smith, and M. H. Mikkelsen, Probing

the mechanisms of large Purcell enhancement in plasmonic nanoantennas, Nat. Photonics **8**, 835 (2014).

[67] K. A. Ivanov, K. M. Morozov, G. Pozina, A. R. Gubaydullin, E. I. Girshova, and M. A. Kaliteevski, Control of the surface plasmon dispersion and Purcell effect at the metamaterial-dielectric interface, Sci. Rep. **10**, 20828 (2020).

[68] D. Turan, P. Keng Lu, N. T. Yardimci, Z. Liu, L. Luo, J. Park, U. Nandi, J. Wang, S. Preu, and M. Jarrahi, Wavelength conversion through plasmon-coupled surface states, Nat. Commun. **12**, 4641 (2021).

[69] M. Khazali, K. Heshami, and C. Simon, Single-photon source based on Rydberg exciton blockade, J. Phys. B: At. Mol. Opt. Phys. **50**, 215301 (2017).

[70] M. Kohlhoff, Interaction of Rydberg atoms with surfaces, Eur. Phys. J. Spec. Top. **225**, 3061 (2016).

[71] K. S. Yee, Numerical solution of initial boundary value problems involving Maxwell's equations in isotropic media, IEEE Trans. Antennas Propagat. **14**, 302 (1966).

[72] A. Taflove, S. C. Hagnes, and M. Piket-May, Computational electrodynamics: The finite-difference time-domain method, in *The Electrical Engineering Handbook*, edited by W.-K. Chen (Elsevier, Burlington, 2005), pp. 629–670.

[73] N. Okada and J. B. Cole, Effective permittivity for FDTD calculation of plasmonic materials, Micromachines **3**, 168 (2012).

[74] J. C. Garrison and R. Y. Chao, *Quantum Optics* (Oxford University Press, Oxford, 2012).

[75] I. S. Gradshteyn and I. M. Ryzhik, *Table of Integrals, Series, and Products*, 5th ed. (Academic Press, London, 1994).

Correction: The Acknowledgment section was missing and has been inserted.